Optics Letters

Polarization discrimination and surface sensing with a near-IR nanostructured hybrid mirror

Oleksandr Buchnev,[1] Alexandr Belosludtsev,[2] and Vassili A. Fedotov[1,*]

[1] Optoelectronics Research Centre and Centre for Photonic Metamaterials, University of Southampton, Southampton SO17 1BJ, UK
[2] Optical Coating Laboratory, Center for Physical Sciences and Technology, Vilnius LT-02300, Lithuania
*Corresponding author: vaf@orc.soton.ac.uk

We demonstrate experimentally how to turn a conventional distributed Bragg reflector into a polarization selecting mirror operating in the near-IR at normal incidence without diffraction and with high extinction ratio. Our approach involves combining a dielectric multilayer composite with a sub-wavelength metal wire-grid nanograting, which can be routinely fabricated using well-established planar fabrication techniques. Moreover, the design and working principle of our nanostructured hybrid mirror enable it to operate as a surface sensor and allow straightforward integration of the mirror with functional materials for tuning its wave-length/polarization extinction ratio.

Polarization is one of the most fundamental characteristics of light in both classical and quantum regimes. Thus, the ability to control (or determine) the polarization state of light is of practical importance to many domains of science and technology, with virtually all applications where light is used (from photography to quantum encryption), relying on such ability. A number of mechanisms are responsibly for perturbing the polarization of light in the course of light–matter interaction, and chief among them is reflection. For example, the handedness of circular polarization is reversed at normal incidence, while linear polarization becomes elliptical at oblique incidence upon reflection [1]. Given that mirrors are hard to avoid in optical systems, as they are widely used for redirecting light or building optical cavities, embedding polarization control in mirrors helps minimize the number of required optical components (and, hence, the size) and improve the efficiency of optical systems. This has become increasingly important with the current drive toward chip-scale optical systems for spectroscopy, sensing, and optical signal processing, not to mention the development of compact light sources based on distributed Bragg reflectors such as, most notably, vertical cavity surface emitting lasers.

One of the actively researched approaches to supplementing mirrors with polarization control involves the use of planar metamaterials (or metasurfaces) – artificially engineered nondiffracting thin films periodically patterned on a sub-wavelength scale. It has enabled the demonstration of the so-called magnetic mirrors [2], chiral and handedness preserving mirrors [3,4], and reflective polarization converters [5,6], to name a few. While such metamaterial-based mirrors offer an unprecedented degree of control over the polarization state of light upon reflection, including tuneability and ultrafast switching of polarization characteristics [7,8], they are generally characterized by low reflectivity levels and are still too challenging to fabricate routinely. From a practical point of view, however, a more favorable approach is to employ wire-grid polarizers in reflection mode. Although their operation is typically limited to linear polarization, they can be highly reflective and exhibit a very high polarization extinction ratio over a wide wavelength range [9–12]. Unfortunately, wire-grid polarizers that would efficiently operate in the near-IR and visible via *zero-order diffraction only* are also difficult to fabricate, as their patterns must have a period of the order of 100 nm (or even less) with wires of the grid resembling high aspect-ratio ridges [13–15].

In this Letter, we address the lack of high-quality nondiffracting mirrors with good polarization capabilities in the near-IR. Our practically viable solution is based on a structured resonant metal-dielectric mirror operating at normal incidence. The design and working principle of the hybrid mirror enable it to operate as a surface sensor and allow straightforward integration of the mirror with functional materials for tuning the mirror's operation wavelength/polarization extinction ratio.

Our hybrid mirror combines a conventional distributed Bragg reflector with a nanopatterned wire-grid [see Fig. 1(a)]. Such a combination allows us to make the best of the two components with their optical functions complementing each other – the Bragg reflector ensures reflectivity levels exceeding 99%, while the wire-grid polarizer acts as a non-diffracting polarization discriminating element. Importantly, as we demonstrate experimentally below, pairing a wire-grid polarizer with a Bragg reflector enables substantial relaxation of the requirements for the period of the grid, its duty factor (wire width/period) and aspect ratio of the wires (height/width), making the design and fabrication of the nanograting a fairly straightforward task.

The distributed Bragg reflector was designed as a stack of alternating 11 high-index layers of niobium pentoxide (Nb_2O_5) with a thickness of 159 nm and 10 low-index layers of silicon dioxide (SiO_2) with a thickness of 246 nm. The design of the Bragg reflector ensured its operation in the near-IR with the photonic bandgap in the wavelength range from 1220 nm to 1660 nm. It was fabricated using a standard procedure, whereby layers of Nb_2O_5 and SiO_2 were deposited in turn on a double-side polished fused silica substrate at room temperature using
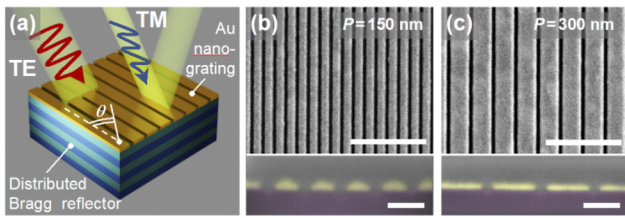
Fig. 1. Polarization-sensitive hybrid metal–dielectric mirror. (a) Schematic of the hybrid mirror interacting with normally incident linearly polarized light. Angle θ shows the azimuth of incident polarization. (b) and (c) SEM images of Au wire-grid nanogratings with periods of 150 nm (duty factor 67%) and 300 nm (duty factor 83%), respectively, fabricated on top of a conventional distributed Bragg reflector. Scale bar is 1 μm. Insets show high-resolution cross sections of the nanogratings in false colors: purple, Nb_2O_5; yellow, Au; gray, Pt (deposited to enhance material contrast). Scale bar is 150 nm.

reactive magnetron sputtering, as detailed in Ref. [16]. The resulting dielectric mirror was terminated by a 50-nm-thick film of gold (Au), which was deposited at room temperature via thermal evaporation of 99.999% purity Au pellets at the rate of 12 nm/min and working pressure of 3.5×10^{-6} Torr. Two wire-grid nanogratings with areas of $30 \times 30 \ \mu m^2$ and periods $P = 150$ nm and $P = 300$ nm were fabricated in the Au film using focused ion beam milling while maintaining the area dose and ion current at typical values of 7 mC/cm^2 and 26 pA, respectively [see Figs. 1(b) and 1(c)]. The slits of the nanogratings were etched all the way through the Au film and had a width of 50 nm, which rendered the wires of the nanogratings as strips with very low aspect ratio. Note, the periods of the two nanogratings were sufficiently sub-wavelength (<540 nm) to ensure no diffraction would occur in both air and dielectric mirror, and at the same time large enough to allow routine fabrication of the nanogratings using common nanolithography techniques (periods < 100 nm are generally challenging to realize).

The polarization selectivity of the samples was examined in reflection at normal incidence for wavelengths in the range 1000–2000 nm using a microspectrophotometer based on a ZEISS Axio microscope. Light was focused onto the samples (and collected) from the Au-coated side of the hybrid mirror using a $\times 15$ Cassegrain-type reflective objective with NA = 0.28. The incident light was linearly polarized with a broadband polarizer incorporating a Glan–Taylor calcite prism. The polarization azimuth, θ, was varied between 0° (TM polarization) and 90° (TE polarization) in steps of 15° by rotating the samples on the rotary stage of the microspectrophotometer. The reflectivity spectra of the samples were acquired from a $22 \times 22 \ \mu m^2$ larger area, as defined by a square aperture installed in the image plane of the instrument.

The reflectivity spectra of the two samples measured for different orientations of incident polarization are shown in Figs. 2(a) and 2(b). Each plot reveals two pronounced reflectivity dips within the photonic bandgap of the Bragg reflector. The dip at a shorter wavelength fully emerges under TE-polarized light and is absent in the case of TM polarization, while its longer-wavelength counterpart exhibits the opposite behavior. Given that the dielectric mirror is totally reflective by design and, at the same time, Au nanogratings are also highly or partially reflective (depending on the polarization), such a strong suppression of the reflectivity by their combination may seem counterintuitive at
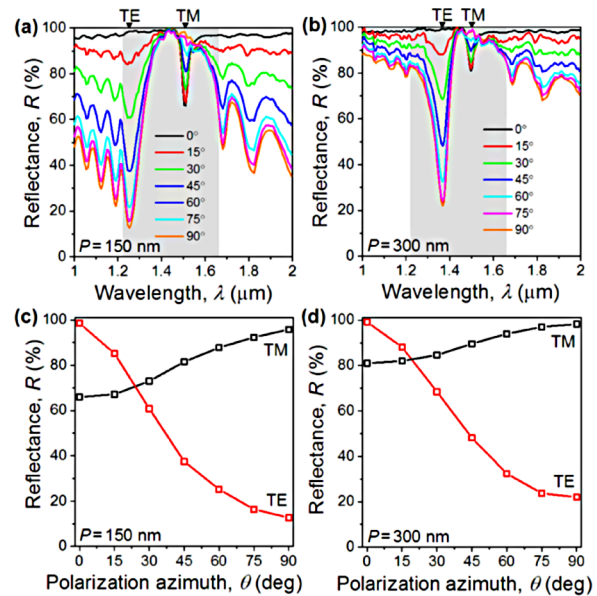

Fig. 2. Polarization discrimination by a hybrid mirror in near-IR. (a) Reflectivity spectra of the hybrid mirror featuring an Au nanograting with 150-nm-long period, measured experimentally for different azimuths of incident polarization. (b) Same as panel (a) but the period of an Au nanograting is 300 nm. Shaded areas mark the extent of the photonic bandgap of a pristine distributed Bragg reflector. (c) Magnitudes of reflectivity dips marked as TM and TE in panel (a), plotted as functions of polarization azimuth. (d) Magnitudes of reflectivity dips marked as TM and TE in panel (b), plotted as functions of polarization azimuth.

first. Hence, next we are going to briefly explain the nature of this effect.

The appearance of the reflectivity dips can be understood if one considers the hybrid mirror as an effective optical cavity formed between the Au film and dielectric Bragg reflector. Such a cavity can support a resonant optical mode (just as any conventional cavity does) provided that the total phase change acquired by light upon completing one round trip inside the cavity is equal to 2π [17]. In the case of a continuous metal film, this mode is known as a Tamm plasmon [17]. A conventional Tamm plasmon forms when an incident optical field tunnels through metal film and becomes trapped at the interface between the film and a Bragg reflector, where its oscillations buildup every round trip due to constructive interference. On resonance, the oscillations grow so strong that when the trapped optical field leaks back through the metal film, its amplitude can become comparable to the amplitude of the primary reflected wave (i.e., the wave reflected directly off the metal film). In this case, the destructive interference of the two waves results in a substantial reduction of the reflectivity, which will occur at the wavelength of Tamm plasmon resonance. Patterning of the metal film on a sub-wavelength scale not only makes it easier for the Tamm plasmon field to leak outside (which results in a broader resonance) but also modifies the dispersion of the reflection phase inside the cavity and, hence, shifts the resonance condition to another wavelength. If the pattern is anisotropic (as in our case), the phase dispersion and, thus, the resonance wavelength will differ for orthogonal polarizations. This is exactly what the spectral plots in Figs. 2(a) and 2(b) show.

While the wavelengths of TE and TM resonances remain fixed, their magnitudes gradually diminish as the azimuth of incident polarization, θ, rotates by 90°. Such a behavior is more apparent in Figs. 2(c) and 2(d). It is characterized by a $\cos^2(\theta)$-like variation typical of linear polarizers and known as the Malus law. We note a slight deviation of the reflectivity level at $\theta = 45°$ from the mean value, which is particularly pronounced for TE resonances. It results from the polarization sensitivity inherent to distributed Bragg reflectors at oblique incidence and is introduced into the measurements via focused illumination of our instrument.

Clearly, Tamm plasmon resonances exhibited by our hybrid reflector render the latter as a highly reflective polarization discriminating mirror. However, a practically usable polarization extinction ratio is achieved only at TE resonances, where it approaches 10:1 in the case of the nanograting with $P = 150$ nm. The large difference between the magnitudes (and, hence, polarization extinction ratios) of TE and TM resonances can be traced back to the transmission characteristics of metallic wire-grid nanogratings. Indeed, nanogratings are naturally more transparent to TE rather than TM polarization and, therefore, they allow the coupling of TE-polarized light into the hybrid cavity at higher rates. As a result, the losses existing in the cavity (chiefly, due to plasmonic dissipation in the metal) are easier to overcome and the oscillations of the Tamm plasmon field can grow stronger than in the case of TM-polarized illumination. This ensures that the Tamm plasmon field that leaks outside interferes destructively to a greater extent with the primary TE-polarized reflected wave, which causes stronger suppression of the reflectivity. By the same token, the reflectivity at the Tamm plasmon resonance will be lower for a nanograting with a shorter period, since it features a larger number of slits and therefore ensures stronger coupling for optical fields. This is why we also observed a pronounced difference between the magnitudes of Tamm plasmon resonances exhibited by the two samples for the same polarization – compare reflectivity dips in Fig. 2 in the case of either TE or TM polarization.

It is worth comparing the efficiency of our polarizing hybrid mirror with that of its *diffracting* counterparts based on high-aspect silicon and metal gratings (see Supplement 1 for an extended comparison). While such gratings also demonstrate a very high base reflectivity of approximately 97% for one polarization, they are unable to suppress the reflectivity for the orthogonal polarization to the same extent as our mirror does. In particular, their cross-polarization reflectivity exceeds 50% if the structure incorporates a silicon grating [18,19] and 40% if the grating is metallic [20]. These levels should be compared to the cross-polarization reflectivities of 12% and 22% characteristics of our mirror, which can be further reduced (increasing the extinction ratio to at least 50:1) via the optimization of nanograting parameters (see Supplement 1).

While the demonstrated concept of a polarization selective hybrid mirror offers several practical advantages, such as non-diffracting operation with high reflectivity in the near-IR and the ease of fabrication using conventional planar techniques, it exploits narrowband optical resonances, the wavelengths of which are fixed by design. We argue, however, that the design and operation principle of the hybrid mirror allow its straightforward integration with functional optical materials which, depending on the application, can be used for either tuning the operation wavelength or modulating the polarization extinction ratio. As a simple illustration of its tuning potential, we demonstrate the
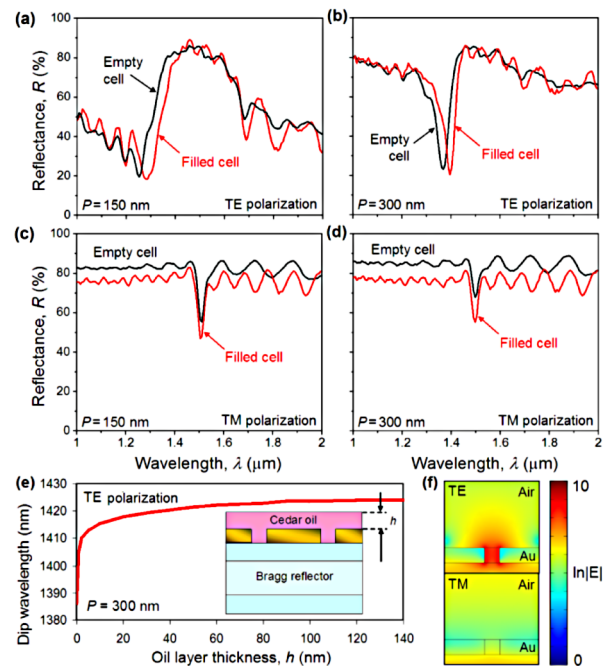

Fig. 3. Tuning operation wavelength of hybrid mirror. (a) Reflectivity spectra of the hybrid mirror featuring an Au nanograting with 150-nm-long period, measured experimentally with TE-polarized light before and after admitting cedar oil. (b) Same as panel (a) but the period is 300 nm. (c) Reflectivity spectra of the hybrid mirror featuring an Au nanograting with 150-nm-long period, measured experimentally with TM-polarized light before and after admitting cedar oil. (d) Same as panel (c) but the period is 300 nm. (e) Wavelength of TE reflectivity dip calculated as a function of oil layer thickness, h. The dependence is modeled for the case of an Au nanograting with a period of 300 nm. Here, $h = 0$ nm corresponds to a pristine hybrid mirror (no oil is present); for any other h, the oil is also filling the slits. (f) Near-field distributions plotted for TE and TM reflectivity dips in the case of $P = 300$ nm.

sensitivity of the hybrid mirror to a change in the ambient refractive index. For this, we integrated the mirror with a plain optical cell, which was then filled with cedar oil (Sigma-Aldrich). The cell was formed by placing a piece of glass slide above the metal-coated side of the Bragg reflector, at a distance of 20 μm away from the metallized surface.

Figure 3 compares the reflectivity spectra of the hybrid mirror before and after filling the optical cell with cedar oil. While the apparent 20% downshift of the reflectivity levels in all cases results from reflection losses and alteration of the optical path within the cell due to focused illumination, there are spectral changes specific only to TE polarization. Indeed, the spectral locations of TM resonances remain virtually unaffected [see Figs. 3(c) and 3(d)], but both TE resonances are seen to undergo a redshift of approximately 30 nm upon admission of the oil [see Figs. 3(a) and 3(b)]. More specifically, the shift is 28 nm when the period of the nanograting, P, is 150 nm and 35 nm when $P = 300$ nm. The pronounced difference between the sensitivities of TE and TM resonances is another manifestation of strong optical-coupling anisotropy inherent to metallic nanogratings. Note, though, that the polarization extinction ratio changed (increased) in all cases upon the admission of oil. This resulted from the increase of optical coupling through the nanoslits, as

they effectively became wider relative to the wavelength (the latter contracts in a dielectric).

Assuming that the refractive index of cedar oil is 1.515, the spectral shifts of TE resonances induced in the two samples translate to the sensitivities of, respectively, 54 nm/RIU and 68 nm/RIU, which are on par with the sensitivities demonstrated in the past for conventional Tamm plasmons [21–23]. This is quite remarkable given that the previously used configurations involved the integration of functional materials into the very structure of distributed Bragg reflectors (by either engineering mesopores or introducing additional layers) and are generally infeasible as a practical implementation of the tuning mechanism. Importantly, in our case, the Tamm plasmon field extends outside the hybrid cavity to a distance comparable to the width of the nanoslits. To confirm the extent of the field, we calculated the wavelength of the reflectivity dip for different thicknesses of the cedar oil layer covering the nanograting [as schematically shown in the inset to Fig. 3(e)]. The calculations were performed using Comsol Multiphysics for TE-polarized plane wave normally incident on an Au nanograting with a period of 300 nm. The obtained dependence shown in Fig. 3(e) indicates that the Tamm plasmon field extends outside the hybrid mirror to a distance of less than 80 nm. In practice, tuning the operation wavelength of our polarization discriminating mirror will require a layer of a functional material significantly thinner than 80 nm, as TE resonance appears to be most sensitive to the first 20 nm of the functional layer. This is also confirmed by modeled distributions of the near field [Fig. 3(f)]. Thus, even though the sensitivity of our hybrid mirror is moderate compared to other sensing approaches [24], the fact that an analyte can be thinner than 20 nm (which is comparable to the size of proteins and viruses) renders our approach as true surface sensing.

The demonstrated approach also offers an easy to implement practical solution for efficient control or stabilization of light polarization in chip-scale optical systems aimed at spectroscopy, optical signal processing, and compact/planarized narrowband light sources such as, for example, vertical cavity surface emitting lasers. In the latter case, to account for a drift of the lasing wavelength, the operation wavelength of our polarizing mirror can be actively tuned with a very thin layer of a functional material, which is sufficient to deposit directly on the surface of the mirror.

In conclusion, we have proposed and experimentally demonstrated a polarization discriminating highly reflective mirror, which operates in the near-IR at normal incidence and *without* diffraction. The mirror is formed by a combination of a conventional distributed Bragg reflector and a 50-nm-tall metallic wire-grid nanograting. The nanograting is characterized by a moderately sub-wavelength period ($\lambda/4.6$–$\lambda/8.3$) and a large duty factor (>0.65), which renders such a nanograting straightforward to mass-produce using mainstream nanolithography techniques, such as e-beam and nanoimprint lithographies, and, recently, laser-induced imprinting of surface periodic structures [25]. The mechanism of the demonstrated polarization discrimination relies on the excitation of Tamm plasmons in the hybrid optical cavity formed by the nanograting and Bragg reflector and admits extending the operation of the mirror to oblique incidence. The polarization extinction ratio achieved in an experiment for linear polarizations is just short of 10:1. Replacing an array of nanoslits forming the nanograting with

concentric nanorings will allow one to extend the mechanism of polarization discrimination to radial and azimuthal polarizations.

Disclosures. The authors declare no conflicts of interest.

Data availability. Following a period of embargo, the data from this paper can be obtained from the University of Southampton repository at Ref. [26] .

Supplemental document. See Supplement 1 for supporting content.

REFERENCES

1. E. Hecht, *Optics*, 3rd ed. (Addison-Wesley Longman, 1998).
2. A. S. Schwanecke, V. A. Fedotov, V. V. Khardikov, S. L. Prosvirnin, Y. Chen, and N. I. Zheludev, J. Opt. A: Pure Appl. Opt. **9**, L1 (2007).
3. E. Plum and N. I. Zheludev, Appl. Phys. Lett. **106**, 221901 (2015).
4. Q. Wang, E. Plum, Q. Yang, X. Zhang, Q. Xu, Y. Xu, J. Han, and W. Zhang, Light: Sci. Appl. **7**, 25 (2018).
5. J. Hao, Y. Yuan, L. Ran, T. Jiang, J. A. Kong, C. T. Chan, and L. Zhou, Phys. Rev. Lett. **99**, 063908 (2007).
6. J. Kim, S. Choudhury, C. DeVault, Y. Zhao, A. V. Kildishev, V. M. Shalaev, A. Alù, and A. Boltasseva, ACS Nano **10**, 9326 (2016).
7. M. Liu, E. Plum, H. Li, S. Duan, S. Li, Q. Xu, X. Zhang, C. Zhang, C. Zou, B. Jin, J. Han, and W. Zhang, Adv. Opt. Mater. **8**, 2000247 (2020).
8. L. Kang, C.-Y. Wang, X. Guo, X. Ni, Z. Liu, and D. H. Werner, Nano Lett. **20**, 2047 (2020).
9. G. R. Bird and M. Parrish, J. Opt. Soc. Am. B **50**, 886 (1960).
10. J. P. Auton, Appl. Opt. **6**, 1023 (1967).
11. P. K. Cheo and C. D. Bass, Appl. Phys. Lett. **18**, 565 (1971).
12. L. G. Josefsson, Ericsson Technics **34**, 181 (1978).
13. D. Kim, Appl. Opt. **44**, 1366 (2005).
14. T. Weber, T. Käsebier, M. Helgert, E.-B. Kley, and A. Tünnermann, Appl. Opt. **51**, 3224 (2012).
15. S. Im, E. Sim, and D. Kim, Sci. Rep. **8**, 14973 (2018).
16. K. Juškevičius, M. Audronis, A. Subačius, S. Kičas, T. Tolenis, R. Buzelis, R. Drazdys, M. Gaspariūnas, V. Kovalevskij, A. Matthews, and A. Leyland, Thin Solid Films **589**, 95 (2015).
17. M. Kaliteevski, I. Iorsh, S. Brand, R. A. Abram, J. M. Chamberlain, A. V. Kavokin, and I. A. Shelykh, Phys. Rev. B **76**, 165415 (2007).
18. T. Moser, H. Glur, V. Romano, F. Pigeon, O. Parriaux, M. A. Ahmed, and T. Graf, Appl. Phys. B **80**, 707 (2005).
19. T. Kämpfe, S. Tonchev, A. V. Tishchenko, D. Gergov, and O. Parriaux, Opt. Express **20**, 5392 (2012).
20. Y. K. Zhong, S. M. Fu, W. M. Huang, D. Rung, J. Y.-W. Huang, P. Parashar, and A. Lin, Opt. Express **25**, A124 (2017).
21. H.-C. Cheng, C.-Y. Kuo, Y.-J. Hung, K.-P. Chen, and S.-C. Jeng, Phys. Rev. Appl. **9**, 064034 (2018).
22. B. Auguie, M. C. Fuertes, P. C. Angelom, N. L. Abdala, G. J. A. A. S. Illia, and A. Fainstein, ACS Photonics **1**, 775 (2014).
23. S. Kumar, M. K. Shukla, P. S. Maji, and R. Das, J. Phys. D: Appl. Phys. **50**, 375106 (2017).
24. Y. Xu, P. Bai, X. Zhou, Y. Akimov, C. E. Png, L.-K. Ang, W. Knoll, and L. Wu, Adv. Opt. Mater. **7**, 1801433 (2019).
25. E. Skoulas, A. C. Tasolamprou, G. Kenanakis, and E. Stratakis, Appl. Surf. Sci. **541**, 148470 (2021).
26. V. Fedotov, "Polarization discrimination and surface sensing with a near-IR nanostructured hybrid mirror," University of Southampton Repository (2022). https://doi.org/10.5258/SOTON/D2294